Volumetric Color Flow Map using Row Column Transducer array - Simulation study

Jørgensen, Lasse Thurmann; Schou, Mikkel; Stuart, Matthias Bo; Jensen, Jørgen Arendt

Published in:
Proceedings of 2018 IEEE International Ultrasonics Symposium

Link to article, DOI:
10.1109/ULTSYM.2018.8580118

Publication date:
2018

Document Version
Peer reviewed version

Volumetric Color Flow Map using Row Column Transducer array - Simulation study.

Lasse Thurmann Jørgensen, Mikkel Schou, Matthias Bo Stuart and Jørgen Arendt Jensen
Center for Fast Ultrasound Imaging, Dept. of Elec. Eng., Bldg. 349, Technical University of Denmark, 2800 Kgs. Lyngby, Denmark

***Abstract*—Volumetric Color Flow Mapping (CFM) is typically performed using matrix probes with up to 9,000 elements. The many elements necessitate the use of highly specialized and expensive probes with dedicated electronics. This paper demonstrates how Row Column Addressed (RCA) transducer arrays can provide volumetric CFM using only 1/72 times the number of elements used for conventional matrix probes without ECG gating. A simulation study is carried out and a constant parabolic vessel flow beneath a 62 + 62 flat surfaced RCA-transducer with a center frequency of 3.5 MHz is simulated. A Synthetic Aperture Focusing Technique (SAFT) is used to construct volumetric images covering a region of $13.2 \times 13.2 \times 48.4$ mm^3 from eight focused emissions. The image lines in the volume are beamformed in parallel, and the axial velocity estimation is performed using eight consecutive realisations of the volumetric image. A volume rate of ~ 234 Hz is reached, with a pulse repetition frequency (f_{prf}) of 15 kHz. From eight center line velocity profiles, the relative mean bias and standard deviation were calculated to be -0.60% and 2.93%, respectively.**

I. Introduction

Fully populated 2-D matrix ultrasound transducers make real-time volumetric imaging possible [1]. A main concern for such a set-up is the number of elements, which increase quadratically with the dimensions of the aperture. The Row Column Addressed (RCA) transducer arrays address this problem by reducing the number of elements from N^2 to $N + N$, while still retaining the 3-D imaging capability of the matrix probe [2] [3].

Two significant bottlenecks facing real-time 3-D ultrasound imaging are the number of electrical connections in the 2-D probe and the $\sim$ 25 Hz frame rate requirement for cardiac imaging [4] [5]. ECG and respiration gating can be employed to circumvent a low volume rate. Here motion artefacts are reduced by tying the acquisition to specific events in the cardiac-/respiratory cycle. This acquisition technique further reduces the volume rate. Synthetic Aperture (SA) systems can be used to address the volume rate problem without ECG gating. Here continuous volumetric images, suitable for velocity estimations [6] can be constructed from an emission sequence that insonifies the volume from different angles. The number of emissions used to create a volumetric image can be kept relatively low using a sparse SA emission scheme and frame rates far exceeding the 25 Hz can potentially be reached. The SA is further discussed in section II-A.

The low channel count of an RCA-transducer reduces the number of electrical connections, eases the manufacturing process of the transducer front end, and allows for much lower data rates from the front end to the processing unit. This shows great potential to overcome problems such as heating in the probe handle, production cost and requirements for the data transfer. The RCA-transducer is addressed through the rows and columns only. The rows and columns can be considered elongated line elements that are positioned orthogonal to each other. The elongated elements give rise to edge artefacts, which have been investigated by Rasmussen et al. [3]. The focused field is obtained by emitting with the row-elements and receiving with the column-elements, and vice versa. The transmitted field, in the plane of the transmit elements, is a focused wave, and is in the dimension of the receive elements, a plane wave. This gives the wave propagation wavefront the geometric shape of a cylinder. By focusing the orthogonal line-elements during receive, information of a specific point in the volume can be obtained through a modified delay-and-sum beamformer [7]. A drawback of the RCA-transducer is related to the edge effects, which cause ghost echoes in the emitted field. These can be reduced by integrating apodization along the length of line-elements [3].

The purpose of this paper is to demonstrate that RCA-transducers can perform volumetric Color Flow Mapping (CFM) with a low standard deviation at a volume rate of ~ 234 Hz. The following section introduces an RCA-transducer acquisition scheme capable of 3-D imaging at a high volume rate. Section III presents an implementation of the acquisition scheme, and Section IV demonstrates its ability to provide volumetric images for velocity estimations.

II. Theory

A. Synthetic Aperture

The image construction is performed using Synthetic Aperture Focusing Technique (SAFT). The basic idea of SA imaging is to gather backscattered data with a different phase and amplitude [8]. After beamformation, the data is summed to create an image with a higher lateral resolution. The acquisition is performed by emitting a cylindrical wave at different origins spanning the physical aperture. Each emission generates a Low Resolution Volume (LRV). The resolution is low because focusing is applied in receive only. Dynamic transmit focusing is synthesized by combining the LRV with an appropriate spatial weighting on the image-points based on the wave propagation path [6].

A high volume rate can be achieved with a sparse synthetic aperture. Using SAFT, a sparse virtual array is constructed

with the focal lines as virtual source points [8]. In this paper, the focused field is emitted by a sliding sub-aperture, with the focal line's lateral position at the center of the sub-aperture, thus creating a linear virtual array. The benefit of the virtual array is an extended depth of focus in the imaging and the increased transmission energy, which equates to an increased penetration depth [9]. One of the concerns related to the sparse virtual array is the grating lobes caused by the often large spacing between the virtual sources. The grating lobes can be reduced by increasing the focal depth, and by virtual source apodization [6].

B. Velocity estimation

The SA flow approach presented by Nikolov and Jensen is used for the velocity estimation [10]. Here the movements of scatters are detected as the lag displacement of the peak in the cross-correlation of two consecutive RF-emissions [11]. The precision of the velocity estimate is multifactorial: the width of the segmentation of the RF-signal, the sampling frequency, the center frequency, pulse repetition frequency (f_{prf}), etc., all affect the likelihood of detecting the correct peak [12]. Three measures were taken to reduce the probability of detecting an erroneous peak. The first was having a search area for the maximum peak, which should be based on the largest velocity expected; the second was averaging several consecutive cross-correlations; and the third was using an unbiased cross-correlation estimator; here the correlogram is divided element-wise with the autocorrelation of the window function used for the segmentation. A benefit of the unbiased estimator is that the expected value is the true cross-correlation value. The cost is, however, an increased variance towards the end-points of the correlogram. The discrete cross-correlation performed using frequency domain multiplication is expressed by:

$$\hat{R} = \sum_{i=1}^{N-1} \mathrm{DFT}^{-1}\Big\{\overline{\mathrm{DFT}}\{s_i\}\mathrm{DFT}\{s_{i+1}\}\Big\}\frac{1}{\sigma_{s_i}\sigma_{s_{i+1}}}, \qquad (1)$$

where s_i denotes a specific segment of the RF-signal at time instant i, N is the number of emissions being averaged, σ_s is the standard deviation of the segment and DFT represents the Discrete Fourier Transform. The standard deviation of the signals correlated are used as a normalization factor ensuring equal weighting of the summed correlograms. Note also that division by $N-1$ is omitted, since only the position of the peak - not its value - is of interest. The lag displacement analysis is performed using arg max:

$$k_d = \underset{k}{\mathrm{argmax}}\big(\hat{R}(k)\big), \qquad (2)$$

where k denotes the lag of the cross-correlation value. To improve the resolution of the lag, a second-order polynomial is fitted to the peak and its neighbouring points. The lag of the interpolated maximum peak is then calculated by [12]:

$$k_{int} = k_d - \frac{\hat{R}(k_d+1) - \hat{R}(k_d-1)}{2\big(\hat{R}(k_d+1) - 2\hat{R}(k_d) + \hat{R}(k_d-1)\big)}. \qquad (3)$$

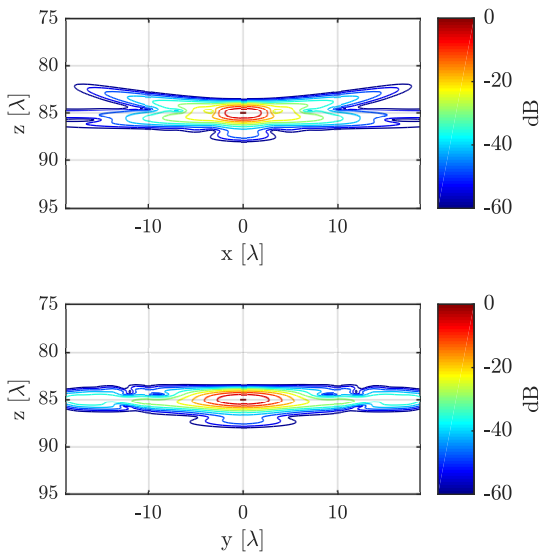

Fig. 1. PSF seen in transmit-plane (bottom) and receive plane (top). The full width half maximum is smaller in the elevation (x) than in the azimuth-dimension (y). The resolution is therefore higher in the receive-plane.

From the lag of the maximum peak, the axial velocity is estimated by the following equation:

$$v = \frac{c}{2}\frac{k_{int} f_{prf,eff}}{f_s}, \qquad (4)$$

where f_s is the sampling frequency and $f_{prf,eff}$ is the effective f_{prf}, which is further discussed in the following section.

III. Method

Volumetric imaging is conducted by emitting a focused wave using the column elements and receiving with all the row elements in parallel. A volume corresponding to the insonified area of the transmitted wave path is then beamformed to a LRV. After N_{vs} emissions, the LRV are summed together to create a High Resolution Volume (HRV). With N realisations of the HRV, the velocities along the beam-direction are estimated using the cross-correlation estimator.

A 62 + 62 linear RCA array with 0.61λ pitch and a center frequency of 3.5 MHz was simulated in Field II [13] [14]. Beneath the transducer, a vessel with constant parabolic flow with 0.1 m/s peak velocity (v_{max}) and a beam-to-flow angle of $60°$ is placed at a depth of $85\lambda = 37.4$ mm. The length axis of the vessel was aligned with the transmitting column elements. The radius of the vessel was set to 6 mm and the length chosen such that its projection onto the aperture plane was 10% longer than the line-elements.

The flow was simulated by translating a collection of uniformly randomly distributed scatters within the boundaries of the vessel. The velocity of the individual scatterers was calculated by:

$$v(r) = \left(1 - \frac{r^2}{R^2}\right) \cdot v_{max}, \qquad (5)$$

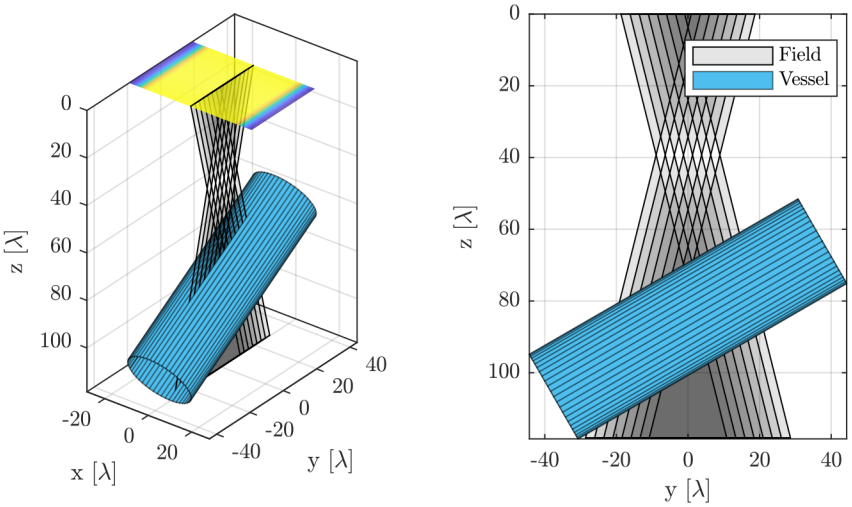

Fig. 2. Simulation set-up seen from two angles. The figure shows the transmit aperture, the vessel and the eight focused fields used to create the HRV. Each field illustrates the wave propagation path of an emission. The lateral resolution is highest in regions where all the fields overlap.

where R is the radius of the vessel and $r \in [0, R]$ is the radial coordinate. The displacement, $\vec{d}(\vec{r})$, at the time of the next emission is then given by:

$$\Delta\vec{d}(\vec{r}) = 1/f_{prf} \cdot \vec{v}(\vec{r}). \tag{6}$$

The emission sequence was simulated by sliding 32 active transmitting elements across the array in steps of $\sim 2.5\lambda$ while receiving with all 62 orthogonal elements in parallel. Beamformation using a sliding aperture yielded image-points covering the full rectilinear volume of $13.2\times13.2\times48.4$ mm^3. The axial velocity was estimated in parallel using $N = 8$ consecutive HRVs and the number of virtual source points to span the aperture was set to $N_{vs} = 8$. The elements of the virtual array were spaced linearly with a pitch equal to the stride of the sliding sub-aperture. A reasonable reduction of the grating lobes in the transmit plane was achieved empirically by applying virtual source apodization and by setting the transmit F-number to 2. The Point Spread Function (PSF) in both the receive, $(x, y, z)|_{y=0}$, and the transmit, $(x, y, z)|_{x=0}$, plane is shown in Fig. 1.

With the described acquisition scheme, $f_{prf,eff}$ is $1/N_{vs}$ times the actual f_{prf}. This reduction is due to the fact that N_{vs} emissions are used to generate an HRV. Though a low $f_{prf,eff}$ is less of an issue for the cross-correlation estimator, since the maximum detectable velocity only is constrained to the maximum lag of the correlogram, rapid de-correlation would still occur at larger velocities. The reduction of $f_{prf,eff}$ necessitates a high f_{prf}, which in turn reduces the visualisation depth. A volume rate of $f_{prf,eff}/N \approx 234$ Hz, with a visualisation depth of about 48.4 mm, was obtained with $f_{prf} = 15$ kHz. The simulation parameters are summarized in table I and the set-up is illustrated in Fig. 2.

TABLE I
SIMULATION PARAMETERS

Transducer	
Parameter	Value
Trandsucer type	2-D Row-Column
Number of elements in x	62
Number of elements in y	62
Pitch in x	0.27 mm = 0.61λ
Pitch in y	0.27 mm = 0.61λ
Width	0.245 mm
Kerf	0.025 mm
Sampling frequency	120 MHz
Center frequency	3.5 MHz
Footprint size	1.67×1.67 cm^2
Sub-element apo.	Tukey
Flow	
Parameter	Value
Flow type	Parabolic
Center Velocity	0.1 m/s
Beam-to-flow angle	60°
Acquisition	
Parameter	Value
Sliding aperture size	32 (transmit)
F# (transmit/receive)	2/1 (dynamic)
Transmit/receive apo.	Hann.
Virtual array apo.	Tukey
Speed of sound	1540 m/s

IV. Results and Discussion

From eight axial velocity profiles of the center line, the relative mean bias and standard deviation (σ) was calculated to be -0.60% and 2.93%. The mean bias and σ were calculated from the central 90% of the velocity profile to exclude potential edge effects. The mean velocity profile $\pm\sigma$ can be seen to closely follow the theoretical profile in Fig. 3. The relative mean bias and σ of the axial velocity profiles in the $(x, y, z)|_{x=0}$ plane is shown in Fig. 4. The mean bias is relatively constant near the center of the aperture but diverges towards the edge; indicating a slight skewing of the vessel structure. The mean σ remain relatively constant throughout the image. 3-D Contour slices of the entire volumetric CFM are shown in Fig. 5. It can be seen that the CFM retains the characteristic of the vessel, and the velocity contours demonstrate a parabolic distribution in the entire volume.

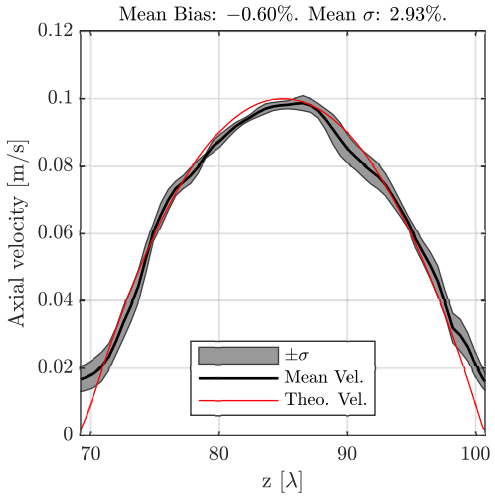

Fig. 3. Black line: Estimated mean axial velocity profile averaged over 8 estimates, gray shading: ± standard deviation of the 8 estimates. Red line: Theoretical mean used to simulate the velocity of the scatters.

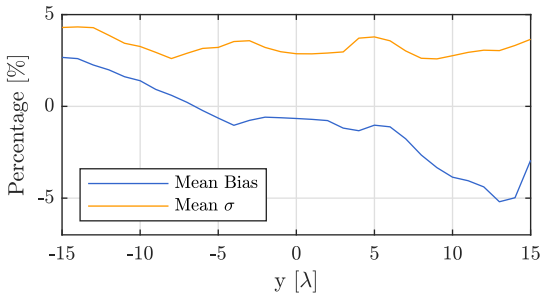

Fig. 4. Orange line: Relative mean standard deviation of the velocity profiles in the $(x, y, z)|_{x=0}$ plane. Blue line: Corresponding relative mean bias of the velocity estimates.

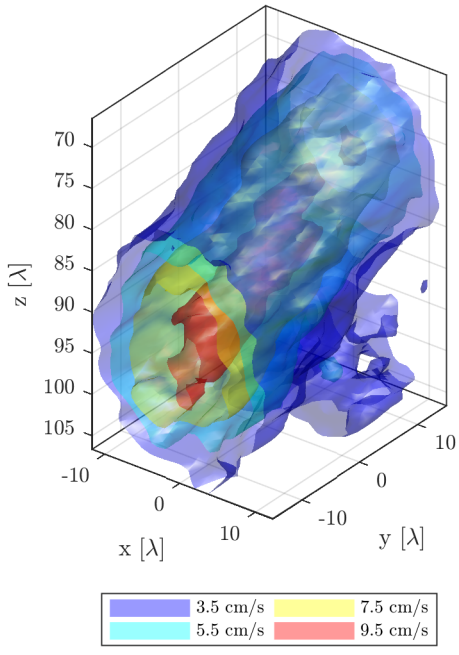

Fig. 5. 3-D contour plot showing axial velocities estimates of the volumetric CFM. Contour limits are shown with different colors.

V. Conclusion

An RCA-transducer ultrasound imaging system able to acquire volumetric images down to 48.4 mm at a volume rate of $\sim$ 234 kHz was presented and simulated in Field II. Using updating after each HRV can yield a volume rate 1875 Hz. The axial velocity of constant parabolic flow in a vessel beneath the transducer was measured, using a cross-correlation estimator. The relative mean bias and standard deviation of eight velocity profiles of the center line, was calculated to -0.60% and 2.93% respectively. Furthermore, a 3-D rendering of the volumetric CFM demonstrates that the estimated velocities are found within the vessel as expected. The parabolic flow distribution is also visible in the 3-D colormap. The SA data acquired in this sequence can also be used in any of the vector flow estimates described in [15] for full 3-D vector flow imaging.

References

[1] O. T. von Ramm, S. W. Smith, and H. G. Pavy, "High speed ultrasound volumetric imaging system – Part II: Parallel processing and image display," *IEEE Trans. Ultrason., Ferroelec., Freq. Contr.*, vol. 38, pp. 109–115, 1991.

[2] C. H. Seo and J. T. Yen, "A 256 x 256 2-D array transducer with row-column addressing for 3-D rectilinear imaging," *IEEE Trans. Ultrason., Ferroelec., Freq. Contr.*, vol. 56, no. 4, pp. 837–847, April 2009.

[3] M. F. Rasmussen, T. L. Christiansen, E. V. Thomsen, and J. A. Jensen, "3-D imaging using row–column-addressed arrays with integrated apodization — Part I: Apodization design and line element beamforming," *IEEE Trans. Ultrason., Ferroelec., Freq. Contr.*, vol. 62, no. 5, pp. 947–958, 2015.

[4] M. Cikes, L. Tong, G. R. Sutherland, and J. D'hooge, "Ultrafast cardiac ultrasound imaging: technical principles, applications, and clinical benefits," *JACC. Cardiovascular imaging*, vol. 7, no. 8, pp. 812–823, 2014.

[5] M. F. Rasmussen and J. A. Jensen, "Comparison of 3-D synthetic aperture phased array ultrasound imaging with parallel beamforming," *IEEE Trans. Ultrason., Ferroelec., Freq. Contr.*, vol. 61, no. 10, pp. 1638–1650, 2014.

[6] J. A. Jensen, S. Nikolov, K. L. Gammelmark, and M. H. Pedersen, "Synthetic aperture ultrasound imaging," *Ultrasonics*, vol. 44, pp. e5–e15, 2006.

[7] T. L. Christiansen, M. F. Rasmussen, J. A. Jensen, and E. V. Thomsen, "Row-column addressed 2-D CMUT arrays with integrated apodization," in *Proc. IEEE Ultrason. Symp.*, 2014, pp. 600–603.

[8] S. Nikolov, J. Kortbek, and J. A. Jensen, "Practical applications of synthetic aperture imaging," in *Proc. IEEE Ultrason. Symp.*, 2010, pp. 350–358.

[9] M. L. Li, W. J. Guan, and P. C. Li, "Improved synthetic aperture focusing technique with application in high-frequency ultrasound imaging," *IEEE Trans. Ultrason., Ferroelec., Freq. Contr.*, vol. 51, no. 1, pp. 63–70, January 2004.

[10] S. I. Nikolov and J. A. Jensen, "In-vivo synthetic aperture flow imaging in medical ultrasound," *IEEE Trans. Ultrason., Ferroelec., Freq. Contr.*, vol. 50, no. 7, pp. 848–856, 2003.

[11] O. Bonnefous and P. Pesqué, "Time domain formulation of pulse-Doppler ultrasound and blood velocity estimation by cross correlation," *Ultrason. Imaging*, vol. 8, pp. 73–85, 1986.

[12] J. A. Jensen, *Estimation of Blood Velocities Using Ultrasound: A Signal Processing Approach*. New York: Cambridge University Press, 1996.

[13] ——, "Field: A program for simulating ultrasound systems," *Med. Biol. Eng. Comp.*, vol. 10th Nordic-Baltic Conference on Biomedical Imaging, Vol. 4, Supplement 1, Part 1, pp. 351–353, 1996.

[14] J. A. Jensen and N. B. Svendsen, "Calculation of pressure fields from arbitrarily shaped, apodized, and excited ultrasound transducers," *IEEE Trans. Ultrason., Ferroelec., Freq. Contr.*, vol. 39, pp. 262–267, 1992.

[15] J. A. Jensen, S. I. Nikolov, A. Yu, and D. Garcia, "Ultrasound vector flow imaging I: Sequential systems," *IEEE Trans. Ultrason., Ferroelec., Freq. Contr.*, vol. 63, no. 11, pp. 1704–1721, 2016.